

A CHEBYSHEV MOVING KRIGING MESHLESS APPROACH FOR BUCKLING ANALYSIS OF MULTILAYER COMPOSITE PLATES

Lieu B. Nguyen 1,*

¹Faculty of Civil Engineering, Ho Chi Minh City University of Technology and Education, Ho Chi Minh City, Vietnam.

Abstract. This paper proposes a new and robust numerical framework for the buckling analysis of multilayer composite plates by integrating the Chebyshev Moving Kriging (CMK) meshfree method with a Third-Order Chebyshev Shear Deformation Theory (TCSDT). The novelty of this study lies in the combined use of Chebyshev polynomials for both interpolation and shear deformation modeling. The TCSDT inherently satisfies the zero-traction boundary condition, thereby eliminating the need for shear correction factors, while the orthogonality and fast convergence of Chebyshev polynomials enhance numerical stability and accuracy compared to traditional polynomial formulations. The governing equations are systematically derived using the principle of virtual work, and the critical buckling loads are obtained through the CMK scheme. Benchmark studies demonstrate that the proposed method not only reproduces results from three-dimensional elasticity theory and established higher-order models with excellent accuracy but also offers improved robustness and efficiency. The findings confirm that the CMK-TCSDT framework provides a reliable and efficient computational tool for analyzing the buckling behavior of laminated composite structures.

Keywords: Chebyshev polynomials; laminated composite plates; higher-order shear deformation theory; meshless approaches.

1. Introduction

Multilayer composite plates have a crucial role in numerous engineering applications and are widely utilized across industries like shipbuilding, aerospace, and civil engineering [1]. Owing to their superior mechanical properties and structural efficiency, laminated composite plates have become indispensable in modern engineering. Their high strength to weight ratios and the stiffness to weight ratios, combined with superior wear resistance and reduced weight characteristics, make them ideal for applications in aerospace, marine, automotive, and civil engineering structures. In addition, their inherent design flexibility-enabled by tailoring stacking sequences, fiber orientations, and layer thicknesses allows engineers to optimize structural performance for specific loading and environmental conditions.

Although three-dimensional elasticity models [2, 3] offer detailed predictions, their high com-

putational cost limits practical application to complex structures. To overcome this limitation, scientists have developed Equivalent Single Layer (ESL) theories [4, 5], which achieve a practical balance between accuracy and effectiveness. With their simple implementation and reliable performance valid for both thin and thick plates, ESL theories have become a preferred tool for analyzing laminated composites. Within the ESL framework, three well-known plate theories have been formulated. cal Plate Theory (CPT), formulated using the Love-Kirchhoff hypotheses, is applicable to thin plates but neglects transverse shear effects. In contrast to CPT [6], the First-Order Shear Deformation Theory (FSDT) accounts for shear deformation and thus improves accuracy for moderately thick plates. However, because FSDT assumes a constant transverse shear strain across the thickness, it becomes inaccurate near the surfaces and requires shear correction factors (SCFs) [7–10], which depend on geometry and material properties. To address these limitations, Higher-Order Shear Deformation Theories (HSDTs) have been acquired. HSDTs eliminate the need for SCFs and provide more accurate predictions of displacements and interlaminar stresses. Numerous HSDT models have been proposed using different functions to represent transverse shear strain and stress distributions through the thickness of plate. Ambartsumian [11] first introduced a polynomial-based HSDT for anisotropic plates, later extended by Reddy [4], Levinson [12], and Reissner [13] using higher-order polynomials for laminated composites. Other formulations, including trigonometric, exponential, and hyperbolic functions, have been presented by Stein [14], Touratier [15], Soldatos [16], Grover [17] and Arya [18], and others [7,19-26] for more complex structures. In this study, Chebyshev polynomials are employed as the shear function due to their orthogonality, recursive nature, and superior numerical stability. These properties enhance convergence and reduce ill-conditioning, offering a reliable alternative to conventional polynomial forms [27,28].

Solving three-dimensional elasticity problems remains challenging due to geometric complexity and computational intensity. This has motivated the development of efficient numerical methods such as the finite element method (FEM), isogeometric analysis (IGA), and meshfree methods. Among these, meshfree methods are particularly effective, allowing flexible modeling with unstructured node distributions and direct calculation of displacements and stress in the physical domain. Unlike FEM and IGA, which are formulated in natural (or parametric) coordinates, meshfree methods operate directly using nodal data defined in global coordinates. Previous studies have commonly utilized the Moving Kriging (MK) shape function for solution approximation. For example, Lam et al. [29] introduced the weak-form MK method for 2D structural analysis. That et al. [30, 31] extended it to study static, dynamic, and buckling responses of FG plates using HSDT and refined plate theories, as well as size-dependent models for FG and carbon nanotube-reinforced nanoplates [32,33]. Nguyen et al. [34] applied an improved MK method to investigate nonlinear static bending and dynamic responses of FGM plates. Additional developments can be found in [35-37].

This study proposes an innovative MK meshfree technique that integrates Chebyshev interpolation with the conventional MK approach. While CMK formulations, like other meshfree approaches, are effective for solving complex problems, they are often computationally demanding. By combining the advantages of radial basis functions (RBFs) and Chebyshev polynomials, the present method substantially improves both accuracy and efficiency. Chebyshev polynomials, known for their fast convergence and numerical stability, outperform traditional polynomials in terms of computational robustness. Furthermore, a Chebyshev Shear Deformation Theory (CSDT) is introduced to capture shear stress variation along the thickness while automatically satisfying the zero-shearstress condition at the plate surfaces. To the best of our knowledge, this is the first study to integrate the Chebyshev Moving Kriging (CMK) approach with third-order Chebyshev Shear Deformation Theory (TCSDT) for buckling analysis of multilaver composite plates. Benchmark comparisons confirm the accuracy and effectiveness of the proposed methodology.

In comparison with other referenced models,

the proposed CMK-TCSDT framework exhibits several advantages. First, the TCSDT inherently satisfies the zero-shear-stress boundary condition at the plate surfaces, eliminating the need for shear correction factors that are required in the First-Order Shear Deformation Theory (FSDT). Second, the use of Chebyshev polynomials improves numerical stability and convergence compared to traditional polynomial-based Higher-Order Shear Deformation Theories (HSDTs). Third, the CMK meshfree interpolation provides flexibility in modeling complex geometries, such as plates with cutouts, without the need for a predefined mesh. On the other hand, a limitation of the present method is its higher computational cost compared to classical FEM-based models, particularly for very large-scale problems. Nevertheless, this tradeoff is justified by the significant improvements in accuracy, robustness, and versatility offered by the proposed approach.

2. Kinematic modeling of plate behavior

The HSDT provides a more accurate representation of the displacement field at any point on the plate, which can be expressed as [38]

$$\tilde{\mathbf{u}}(x,y,z) = \mathbf{u}^{1}(x,y) + z\mathbf{u}^{2}(x,y) + f(z)\mathbf{u}^{3}(x,y)$$
(1)

where

$$\tilde{\mathbf{u}} = \begin{Bmatrix} \tilde{u} \\ \tilde{v} \\ \tilde{w} \end{Bmatrix}; \ \mathbf{u}^1 = \begin{Bmatrix} u \\ v \\ w \end{Bmatrix};$$
$$\mathbf{u}^2 = \begin{Bmatrix} \psi_x \\ \psi_y \\ 0 \end{Bmatrix}; \ \mathbf{u}^3 = \begin{Bmatrix} \phi_x \\ \phi_y \\ 0 \end{Bmatrix}$$
 (2)

where u, v, and w imply the displacements along the x, y, and z directions, respectively; while ϕ_x and ϕ_y represent two rotations of the y-z plane and x-z plane, respectively; $\psi_x=w_{,x}=\frac{\partial w}{\partial x}$; $\psi_y=w_{,y}=\frac{\partial w}{\partial y}$. The parameter h is the plate thickness.

The function f(z) characterizes the variation of shear stress along the plate's thickness direction. Within the HSDT framework, different plate theories emerge by selecting specific forms of f(z), such as polynomial [39,40], trigonometric [15, 19, 41], exponential [21, 42], and hyperbolic [22, 43] functions, as summarized in Table 1. In this study, we present an innovative use of the Chebyshev polynomial function. This study introduces the function, denoting p the polynomial order. For illustrative purposes, the third-order case (p=3) is adopted. The proposed formulation inherently satisfies the zero transverse shear stress boundary condition at both the top and bottom plate surfaces, as illustrated in Table 1 and Figure 1. The bending and shear

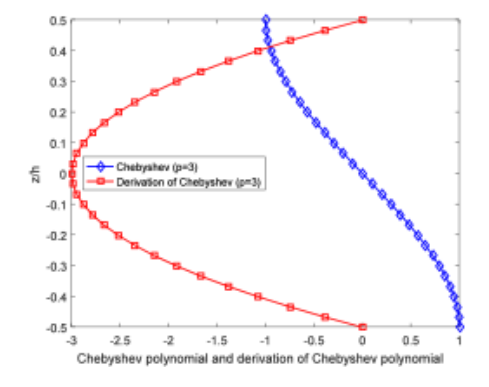


Fig. 1: Characteristics and derivation of Chebyshev Polynomials (p = 3).

deformation terms can be written as follows

$$\boldsymbol{\varepsilon} = \left\{ \varepsilon_{xx} \quad \varepsilon_{yy} \quad \gamma xy \right\}^{\top} = \boldsymbol{\varepsilon}^{1} + z\boldsymbol{\varepsilon}^{2} + f(z)\boldsymbol{\varepsilon}^{3},$$

$$\boldsymbol{\gamma} = \left\{ \gamma_{xz} \quad \gamma_{yz} \right\}^{\top} = \boldsymbol{\varepsilon}^{s1} + f'(z)\boldsymbol{\varepsilon}^{s2}$$
(3)

in which

$$\epsilon^{1} = \begin{Bmatrix} u_{,x} \\ v_{,y} \\ u_{,y} + v_{,x} \end{Bmatrix}, \epsilon^{2} = \begin{Bmatrix} \psi_{x,x} \\ \psi_{y,y} \\ \psi_{x,y} + \psi_{y,x} \end{Bmatrix},$$

$$\epsilon^{3} = \begin{Bmatrix} \phi_{x,x} \\ \phi_{y,y} \\ \phi_{x,y} + \phi_{y,x} \end{Bmatrix}, \epsilon^{s1} = \begin{Bmatrix} w_{,x} - \psi_{x} \\ w_{,y} - \psi_{y} \end{Bmatrix},$$

$$\epsilon^{s2} = \begin{Bmatrix} \phi_{x} \\ \phi_{y} \end{Bmatrix}, f'(z) = \frac{\mathrm{d}f(z)}{\mathrm{d}z}.$$
(4)

The constitutive stress–strain relation for the kth layer of an orthotropic laminate in its local

Kinds	f(z)	Theories
Polynomial functions		
Reddy [39]	$f(z) = z - 4z^3/3h^2$	TSDT (third order)
Nguyen-Xuan et al. [40]		HSDT (fifth order)
Present	$f(z) = \cos(3 \times \cos^{-1}(z/h))$	TCSDT (Third-order Chebyshev)
Trigonometric functions		
Arya et al. [41]	$f(z) = \sin\left(\frac{\pi z}{h}\right)$	TrSDT (Trigonometric shear deformation theory)
Touratier [15]	$f(z) = \frac{h}{2} \sin\left(\frac{\pi z}{h}\right)$	TrSDT
Thai et al. [19]	$f(z) = \tilde{h} \tan^{-1} \left(\frac{2z}{h}\right) - z$	TrSDT
Exponential functions		
Karama et al. [21]	$f(z) = z \times e^{-2\left(\frac{z}{h}\right)^2}$	ESDT (Exponential shear deformation theory)
Mantari et al. [42]	$f(z) = z \times 2.85e^{-2\left(\frac{z}{h}\right)^2} + 0.028z$	ESDT
Hyperbolic functions		
Soldatos [22]	$f(z) = h \sinh\left(\frac{h}{z}\right) - z \cosh\left(\frac{1}{2}\right)$	HySDT (Hyperbolic shear deformation theory)
Thai et al. [43]	$f(z) = \sinh^{-1}\left(\sin\left(\frac{\pi z}{k}\right)\right)$	HvSDT

Tab. 1: Mathematical formulations characterizing the variation of shear stress in the transverse direction through the plate thickness.

coordinate system is given

$$\begin{pmatrix}
\sigma_{xx} \\
\sigma_{yy} \\
\tau_{xy} \\
\tau_{yz}
\end{pmatrix}^{(k)} \begin{bmatrix}
C_{11} & C_{12} & 0 & 0 & 0 \\
C_{21} & C_{22} & 0 & 0 & 0 \\
0 & 0 & C_{66} & 0 & 0 \\
0 & 0 & 0 & C_{55} & 0 \\
0 & 0 & 0 & 0 & C_{44}
\end{bmatrix}^{(k)} \begin{cases}
\varepsilon_{xx} \\
\varepsilon_{yy} \\
\gamma_{xy} \\
\gamma_{xz} \\
\gamma_{yz}
\end{cases}^{(k)}$$
mapped into the global coordinate system. A detailed explanation of these transformed coefficients can be found in Ref. [1].

where $C_{ij}^{(k)}$ is formulated by

$$\begin{split} C_{11}^{(k)} &= \frac{E_1^{(k)}}{1 - \nu_{12}^{(k)} \nu_{21}^{(k)}}, \ C_{12}^{(k)} &= \frac{\nu_{12}^{(k)} E_2^{(k)}}{1 - \nu_{12}^{(k)} \nu_{21}^{(k)}}, \\ C_2^{(k)} &= \frac{E_2^{(k)}}{1 - \nu_{12}^{(k)} \nu_{21}^{(k)}}, \ C_{66}^{(k)} &= G_{12}^{(k)}, \\ C_{55}^{(k)} &= G_{13}^{(k)}, \ C_{44}^{(k)} &= G_{23}^{(k)}. \end{split} \tag{6}$$

Here $E_1^{(k)}$ and $E_2^{(k)}$ are the Young's moduli along the local 1 and 2 axes, respectively; $G_{12}^{(k)}$, $G_{23}^{(k)}$, $G_{13}^{(k)}$ correspond to the shear modeli in the 1-2 2–3, and 1–3 planes, respectively; and $\nu_{12}^{(k)}$, $\nu_{21}^{(k)}$ indicate the Poisson's ratios relating strains in the 1 and 2 directions, respectively.

plates, multilayer composite the stress-strain relations of each kth layer are required to undergo transformation from the local coordinate system to the global coordinate system. This transformation is expressed as

$$\begin{cases} \begin{array}{c} \sigma_{xx}^{(k)} \\ \sigma_{yy}^{(k)} \\ \tau_{xy}^{(k)} \\ \tau_{yz}^{(k)} \\ \end{array} \\ = \begin{bmatrix} \hat{C}_{11}^{(k)} & \hat{C}_{12}^{(k)} & \hat{C}_{16}^{(k)} & 0 & 0 \\ \hat{C}_{21}^{(k)} & \hat{C}_{22}^{(k)} & \hat{C}_{26}^{(k)} & 0 & 0 \\ \hat{C}_{61}^{(k)} & \hat{C}_{62}^{(k)} & \hat{C}_{66}^{(k)} & 0 & 0 \\ 0 & 0 & 0 & \hat{C}_{55}^{(k)} & \hat{C}_{54}^{(k)} \\ 0 & 0 & 0 & \hat{C}_{45}^{(k)} & \hat{C}_{44}^{(k)} \end{bmatrix} \begin{cases} \varepsilon_{xx}^{(k)} \\ \varepsilon_{xy}^{(k)} \\ \varepsilon_{xy}^{(k)} \\ \gamma_{xy}^{(k)} \\ \gamma_{xz}^{(k)} \\ \gamma_{yz}^{(k)} \end{cases} \\ \nabla^{\top} = \begin{bmatrix} \frac{\partial}{\partial x} & \frac{\partial}{\partial y} \end{bmatrix}^{\top}; \ \mathbf{N}_{0} = \begin{bmatrix} N_{x} & N_{xy} \\ N_{xy} & N_{y} \end{bmatrix} \end{cases}$$

$$\mathbf{v}^{\text{there } (i, j = 1)^{t}}$$

$$\nabla^{\top} = \begin{bmatrix} \frac{\partial}{\partial x} & \frac{\partial}{\partial y} \end{bmatrix}^{\top}; \ \mathbf{N}_{0} = \begin{bmatrix} N_{x} & N_{xy} \\ N_{xy} & N_{y} \end{bmatrix}$$

$$\mathbf{v}^{\text{there } (i, j = 1)^{t}}$$

$$\nabla^{\top} = \begin{bmatrix} \frac{\partial}{\partial x} & \frac{\partial}{\partial y} \end{bmatrix}^{\top}; \ \mathbf{v}^{\mathbf{v}} = \begin{bmatrix} N_{x} & N_{xy} \\ N_{xy} & N_{y} \end{bmatrix}$$

$$\mathbf{v}^{\mathbf{v}} = \begin{bmatrix} \frac{\partial}{\partial x} & \frac{\partial}{\partial y} \end{bmatrix}^{\top}; \ \mathbf{v}^{\mathbf{v}} = \begin{bmatrix} \frac{\partial}{\partial x} & \frac{\partial}{\partial y} \end{bmatrix}^{\top}; \ \mathbf{v}^{\mathbf{v}} = \begin{bmatrix} N_{x} & N_{xy} \\ N_{xy} & N_{y} \end{bmatrix}$$

$$\mathbf{v}^{\mathbf{v}} = \begin{bmatrix} \frac{\partial}{\partial x} & \frac{\partial}{\partial y} \end{bmatrix}^{\top}; \ \mathbf{v}^{\mathbf{v}} = \begin{bmatrix} \frac{\partial}{\partial x} & \frac{\partial}{\partial y} \end{bmatrix}^{\top}; \ \mathbf{v}^{\mathbf{v}} = \begin{bmatrix} \frac{\partial}{\partial x} & \frac{\partial}{\partial y} \end{bmatrix}^{\top}; \ \mathbf{v}^{\mathbf{v}} = \begin{bmatrix} \frac{\partial}{\partial x} & \frac{\partial}{\partial y} \end{bmatrix}^{\top}; \ \mathbf{v}^{\mathbf{v}} = \begin{bmatrix} \frac{\partial}{\partial x} & \frac{\partial}{\partial y} \end{bmatrix}^{\top}; \ \mathbf{v}^{\mathbf{v}} = \begin{bmatrix} \frac{\partial}{\partial x} & \frac{\partial}{\partial y} \end{bmatrix}^{\top}; \ \mathbf{v}^{\mathbf{v}} = \begin{bmatrix} \frac{\partial}{\partial x} & \frac{\partial}{\partial y} \end{bmatrix}^{\top}; \ \mathbf{v}^{\mathbf{v}} = \begin{bmatrix} \frac{\partial}{\partial x} & \frac{\partial}{\partial y} \end{bmatrix}^{\top}; \ \mathbf{v}^{\mathbf{v}} = \begin{bmatrix} \frac{\partial}{\partial x} & \frac{\partial}{\partial y} \end{bmatrix}^{\top}; \ \mathbf{v}^{\mathbf{v}} = \begin{bmatrix} \frac{\partial}{\partial x} & \frac{\partial}{\partial y} \end{bmatrix}^{\top}; \ \mathbf{v}^{\mathbf{v}} = \begin{bmatrix} \frac{\partial}{\partial x} & \frac{\partial}{\partial y} \end{bmatrix}^{\top}; \ \mathbf{v}^{\mathbf{v}} = \begin{bmatrix} \frac{\partial}{\partial x} & \frac{\partial}{\partial y} \end{bmatrix}^{\top}; \ \mathbf{v}^{\mathbf{v}} = \begin{bmatrix} \frac{\partial}{\partial x} & \frac{\partial}{\partial y} \end{bmatrix}^{\top}; \ \mathbf{v}^{\mathbf{v}} = \begin{bmatrix} \frac{\partial}{\partial x} & \frac{\partial}{\partial y} \end{bmatrix}^{\top}; \ \mathbf{v}^{\mathbf{v}} = \begin{bmatrix} \frac{\partial}{\partial x} & \frac{\partial}{\partial y} \end{bmatrix}^{\top}; \ \mathbf{v}^{\mathbf{v}} = \begin{bmatrix} \frac{\partial}{\partial x} & \frac{\partial}{\partial y} \end{bmatrix}^{\top}; \ \mathbf{v}^{\mathbf{v}} = \begin{bmatrix} \frac{\partial}{\partial x} & \frac{\partial}{\partial y} \end{bmatrix}^{\top}; \ \mathbf{v}^{\mathbf{v}} = \begin{bmatrix} \frac{\partial}{\partial x} & \frac{\partial}{\partial y} \end{bmatrix}^{\top}; \ \mathbf{v}^{\mathbf{v}} = \begin{bmatrix} \frac{\partial}{\partial x} & \frac{\partial}{\partial y} \end{bmatrix}^{\top}; \ \mathbf{v}^{\mathbf{v}} = \begin{bmatrix} \frac{\partial}{\partial x} & \frac{\partial}{\partial y} \end{bmatrix}^{\top}; \ \mathbf{v}^{\mathbf{v}} = \begin{bmatrix} \frac{\partial}{\partial x} & \frac{\partial}{\partial y} \end{bmatrix}^{\top}; \ \mathbf{v}^{\mathbf{v}} = \begin{bmatrix} \frac{\partial}{\partial x} & \frac{\partial}{\partial y} & \frac{\partial}{\partial y} \end{bmatrix}^{\top}; \ \mathbf{v}^{\mathbf{v}} = \begin{bmatrix} \frac{\partial}{\partial x} & \frac{\partial}{\partial y} & \frac{\partial}{$$

where $\hat{C}_{ij}^{(k)}$ refers to the elastic parameters mapped into the global coordinate system. A

lation of a plate under in-plane loading is given

$$\int_{\Omega} \delta \bar{\mathbf{c}}^T \mathbf{Q}^b \bar{\mathbf{c}} d\Omega + \int_{\Omega} \delta \bar{\boldsymbol{\gamma}}^T \mathbf{Q}^s \bar{\boldsymbol{\gamma}} d\Omega + h \int_{\Omega} \nabla^T \delta w \mathbf{N}_0 \nabla w d\Omega = \mathbf{0}$$
(8)

$$\bar{\boldsymbol{\varepsilon}} = \left\{ \begin{array}{c} \boldsymbol{\varepsilon}^{1} \\ \boldsymbol{\varepsilon}^{2} \\ \boldsymbol{\varepsilon}^{3} \end{array} \right\}, \ \bar{\boldsymbol{\gamma}} = \left\{ \begin{array}{c} \boldsymbol{\varepsilon}^{s1} \\ \boldsymbol{\varepsilon}^{s2} \end{array} \right\},$$

$$\mathbf{Q}^{b} = \left[\begin{array}{ccc} \mathbf{A}^{b} & \mathbf{B}^{b} & \mathbf{E}^{b} \\ \mathbf{B}^{b} & \mathbf{D}^{b} & \mathbf{F}^{b} \\ \mathbf{E}^{b} & \mathbf{F}^{b} & \mathbf{H}^{b} \end{array} \right], \ \mathbf{Q}^{s} = \left[\begin{array}{ccc} \mathbf{A}^{s} & \mathbf{B}^{s} \\ \mathbf{B}^{s} & \mathbf{D}^{s} \end{array} \right]$$

$$(9)$$

$$\begin{split} (A^b_{ij}, B^b_{ij}, D^b_{ij}, E^b_{ij}, F^b_{ij}, H^b_{ij}) \\ &= \int_{-h/2}^{h/2} \left(1, z, z^2, f(z), z f(z)\right) C^k_{ij} \mathrm{dz} \end{split}$$

where (i, j = 1, 2, 6)

$$(A_{ij}^{s}, B_{ij}^{s}, D_{ij}^{s}) = \int_{-h/s}^{h/2} (1, f'(z), f^{'2}(z)) C_{ij}^{k} dz$$

where (i, j = 4, 5)

$$abla^{ op} = \begin{bmatrix} rac{\partial}{\partial x} & rac{\partial}{\partial y} \end{bmatrix}^{ op}; \ \mathbf{N}_0 = \begin{bmatrix} N_x & N_{xy} \\ N_{xy} & N_y \end{bmatrix}$$

where Ω denotes the area of the plate's midsurface.

3. Meshfree interpolation function using Chebyshev moving Kriging approach

To construct the Moving Kriging (MK) interpolation, the neutral surface of the plate (Ω is discretized into a number of nodal points \mathbf{x}_I , where $I=1,2,\ldots,N$ and N denotes the entire set of nodes. Based on this discretization, the displacement field over the plate can be approximated by

$$\mathbf{u}^{h}(\mathbf{x}) = \sum_{I=1}^{N} \mathbf{I}_{7 \times 7} N_{I}(\mathbf{x}) \mathbf{q}_{I}$$
 (10)

in which the degrees of freedom (DOFs) of node I are given by $\mathbf{q}_I = \left\{u_I \quad v_I \quad w_I \quad \phi_{xI} \quad \phi_{yI} \quad \psi_{xI} \quad \psi_{yI}\right\}^{\top}$ and MK interpolation shape function is expressed as

$$N_{I}(\mathbf{x}) = \mathbf{p}^{\top}(\mathbf{x})\mathbf{A} + \mathbf{r}^{\top}(\mathbf{x})\mathbf{B}$$
$$= \sum_{j=1}^{m} p_{j}(\mathbf{x})A_{jI} + \sum_{k=1}^{n} r_{k}(\mathbf{x})B_{kI}$$
(11)

Here, n indicates the number of nodes within the considered domain, and m is the total of the polynomial terms. The following terms are defined as:

$$\mathbf{p}(\mathbf{x}) = \begin{bmatrix} p_1(\mathbf{x}) & p_2(\mathbf{x}) & \cdots & p_m(\mathbf{x}) \end{bmatrix}^{\top}$$

$$\mathbf{r}(\mathbf{x}) = \begin{bmatrix} R(\mathbf{x}_1, \mathbf{x}) & R(\mathbf{x}_2, \mathbf{x}) & \cdots & R(\mathbf{x}_n, \mathbf{x}) \end{bmatrix}^{\top}$$

$$\mathbf{A} = (\mathbf{P}^{\top} \mathbf{R}^{-1} \mathbf{P})^{-1}, \ \mathbf{B} = \mathbf{R}^{-1} (\mathbf{I} - \mathbf{P} \mathbf{A})$$
(12)

where **I** is the identity matrix of $n \times n$ and

$$\mathbf{P}(\mathbf{x}) = \begin{bmatrix} p_1(\mathbf{x}_1) & \cdots & p_m(\mathbf{x}_1) \\ \vdots & \ddots & \vdots \\ p_1(\mathbf{x}_n) & \cdots & p_m(\mathbf{x}_n) \end{bmatrix}, \\ \mathbf{R}(\mathbf{x}) = \begin{bmatrix} R(\mathbf{x}_1, \mathbf{x}_1) & \cdots & R(\mathbf{x}_1, \mathbf{x}_n) \\ \vdots & \ddots & \vdots \\ R(\mathbf{x}_n, \mathbf{x}_1) & \cdots & R(\mathbf{x}_n, \mathbf{x}_n) \end{bmatrix}$$
(13)

The components of $\mathbf{p}(\mathbf{x})$ and $R(\mathbf{x}_i, \mathbf{x}_j)$ are further described by

$$\mathbf{p}(\mathbf{x}) = \left\{ \underbrace{\frac{1 \quad x \quad y \quad x^2 \quad xy \quad y^2}{m=6}} \right\}^{\top},$$

$$R(\mathbf{x}_i, \mathbf{x}_j) = \exp\left\{ -\left(\frac{\eta}{d_c} \|\mathbf{x}_i - \mathbf{x}_j\|\right)^2 \right\}$$
(14)

with η is the correlation parameter ($\eta = 1$) [44], and d_c is represents the average nodal spacing.

In this study, a new interpolation method is proposed by combining radial basis functions (RBFs) with Chebyshev polynomials. By substituting the conventional polynomial terms with Chebyshev polynomials, the resulting Chebyshev Moving Kriging (CMK) interpolation significantly enhances the accuracy of displacement field approximations. The formulation begins with the one-dimensional Chebyshev polynomial defined as

$$C_p(x) = \cos(p \times \cos^{-1}(x)), \ p = 0, 1, 2, \dots$$
(15)

where p denotes the polynomial degree.

Utilizing the orthogonality condition, the traditional polynomial terms in Eq. (13) are replaced by two-dimensional Chebyshev polynomials, expressed as

$$\mathbf{P}(\mathbf{x}) = \begin{bmatrix} C_0(x_1) C_0(y_1) & \cdots & C_p(x_1) C_q(y_1) \\ \vdots & \ddots & \vdots \\ C_0(x_n) C_0(y_n) & \cdots & C_p(x_n) C_q(y_n) \end{bmatrix}_{n \times m}$$

$$(16)$$

where q denotes the Chebyshev polynomial's order in the y-direction, and m is the total sum of the Chebyshev polynomial's terms, as expressed by $m = (p+1) \times (q+1)$.

In this work, only the first derivative of the CMK is required. Therefore, a simplified form based on the second-order Chebyshev polynomial is adopted. This choice provides a balance between computational efficiency and accuracy. Accordingly, m is assigned the value of $9 \ (m = (2+1) \times (2+1))$.

Based on the CMK interpolation shape functions, the relationship between in-plane and shear strains and the displacement field is obtained by substituting Eq. (10) into Eq. (4) as

$$\bar{\varepsilon} = \sum_{I=1}^{N} \bar{\mathbf{B}}_{I}^{b} \mathbf{q}_{I}, \ \bar{\gamma} = \sum_{I=1}^{N} \bar{\mathbf{B}}_{I}^{s} \mathbf{q}_{I}$$
 (17)

The corresponding displacement derivatives are given by

$$\begin{cases} w_{,x} \\ w_{,y} \end{cases} = \sum_{I=1}^{N} \mathbf{B}_{I}^{g} \mathbf{q}_{I} \tag{18}$$

where

$$\mathbf{B}_{I}^{1} = \begin{bmatrix} N_{I,x} & 0 & 0 & 0 & 0 & 0 & 0 \\ 0 & N_{I,y} & 0 & 0 & 0 & 0 & 0 \\ N_{I,y} & N_{I,x} & 0 & 0 & 0 & 0 & 0 \end{bmatrix},$$

$$\mathbf{B}_{I}^{2} = -\begin{bmatrix} 0 & 0 & 0 & 0 & 0 & N_{I,x} & 0 \\ 0 & 0 & 0 & 0 & 0 & N_{I,y} & N_{I,y} \\ 0 & 0 & 0 & 0 & N_{I,y} & N_{I,x} \end{bmatrix},$$

$$\mathbf{B}_{I}^{3} = \begin{bmatrix} 0 & 0 & 0 & N_{I,x} & 0 & 0 & 0 \\ 0 & 0 & 0 & 0 & N_{I,y} & 0 & 0 \\ 0 & 0 & 0 & N_{I,y} & N_{I,x} & 0 & 0 \end{bmatrix},$$

$$\mathbf{B}_{I}^{s1} = \begin{bmatrix} 0 & 0 & N_{I,x} & 0 & 0 & -N_{I} & 0 \\ 0 & 0 & N_{I,y} & 0 & 0 & 0 & -N_{I} \end{bmatrix}$$

$$\mathbf{B}_{I}^{s2} = \begin{bmatrix} 0 & 0 & 0 & N_{I} & 0 & 0 & 0 \\ 0 & 0 & 0 & 0 & N_{I} & 0 & 0 & 0 \\ 0 & 0 & 0 & 0 & N_{I} & 0 & 0 & 0 \end{bmatrix},$$

$$\mathbf{B}_{I}^{g} = \begin{bmatrix} 0 & 0 & N_{I,x} & 0 & 0 & 0 & 0 \\ 0 & 0 & N_{I,y} & 0 & 0 & 0 & 0 & 0 \end{bmatrix}$$

$$(19)$$

Now, we can express the ending equations for the buckling investigation of laminated composite plates as follows:

$$(\mathbf{K} - \lambda_{cr} \mathbf{K}_a) \,\bar{\mathbf{q}} = \mathbf{0} \tag{20}$$

where \mathbf{K}, \mathbf{K}_g , and represent the global stiffness matrix, the geometric stiffness matrix, and the critical buckling value, respectively and are formulated as

$$\mathbf{K} = \int_{\Omega} (\bar{\mathbf{B}}^b)^T \mathbf{Q}^b \bar{\mathbf{B}}^b d\Omega + \int_{\Omega} (\bar{\mathbf{B}}^s)^T \mathbf{Q}^s \bar{\mathbf{B}}^s d\Omega,$$
$$\mathbf{q} = \bar{\mathbf{q}} e^{i\omega t}, \ \mathbf{K}_g = h \int_{\Omega} (\mathbf{B}^g)^\top \mathbf{N}_0 \mathbf{B}^g d\Omega$$
(21)

4. Results

In this section, a series of benchmark problems are conducted to evaluate the efficiency and accuracy of the proposed method for laminated composite plates. The test cases encompass both square plates and plates with complex cutouts, incorporating diverse fiber orientation angles and a wide range of span-to-thickness ratios (a/h). Each laminate is composed of equal thickness and identical linear-elastic composite material. For numerical integration, three-node triangular elements are employed in conjunction with a (3×3) Gaussian quadrature scheme.

4.1. Square plates

1) Square plate subjected to uniaxial compressive loading

In the first case, a four-layer $(0^0/90^0/90^0/0^0)$ laminated square plate with simply supported edges under axial compressive loading is examined. The critical load factor for the plate is expressed as $\bar{\lambda} = \lambda_{cr} a^2/(E_2 h^3)$ where λ_{cr} , a, E_2 , and h correspond to the buckling load at instability, the structural length, the material's elastic modulus along the second axis, and the plate's thickness, respectively. The parameters of the material are $E_1 = 40E_2$, $G_{12} = G_{12} =$ $0.6E_2$, $G_{23} = 0.5E_2$, $\nu_{12} = 0.25$. The plate is modeled by 588 nodes, as shown in Figure 2. Figure 3 illustrates the geometric model of laminated composite plates subjected to both uniaxial and biaxial compression. The influence of different a/h and E_1/E_2 ratios is analyzed. A constant length-to-thickness ratio of a/h = 10is considered, while the elastic modulus ratio E_1/E_2 is varied. Table 2 compares the present results with several reference solutions, including the three-dimensional elasticity solution [45], the Radial Point Interpolation Method (RPIM) with HSDT [46], Isogeometric Analysis (IGA) incorporating trigonometric shear deformation theories (TrSDTs) [41], FEM based on HSDT [47], IGA based on FSDT [48], and a meshfree approach employing Naturally Stabilized Nodal Integration (NSNI) using HSDT [44]. The numerical results exhibit excellent agreement with these established methods, validating its accuracy. As shown in Table 2, the non-dimensional critical buckling load consistently increases with higher values of the modulus ratio E_1/E_2 . This trend reflects the enhanced stiffness in the fiber direction, which improves structural stability. The results are consistent with the expected mechanical behavior of laminated composites, where increasing anisotropy improves resistance to buckling under axial loading.

The following analysis explores how variations in the span-to-thickness ratio (a/h) influence the buckling performance of simply supported square plates with two and four laminae. Table 3 presents the normalized buckling load factors for various a/h values. The results show excellent agreement with those obtained from established methods, including FEM using FEM-FSDT [49], FEM-HSDT [47], IGA-TrSDTs [41], NSNI-HSDT [44], IGA-FSDT [48], and the MISQ20 quadrilateral element [50]. As expected, the normalized buckling load factor increases with larger a/h, confirming the robustness and accuracy of the present approach.

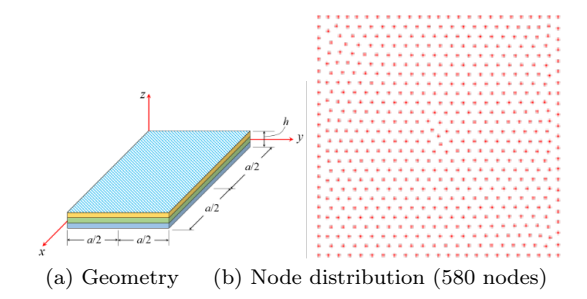


Fig. 2: Geometry and node distribution of square plate.

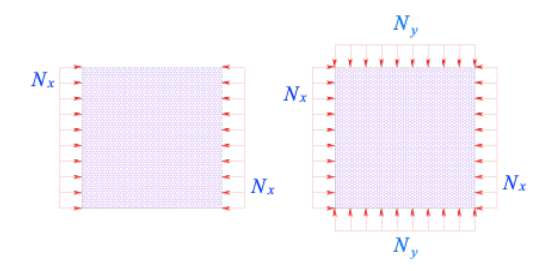


Fig. 3: Configuration of multilayer composite plates subjected to uniaxial and biaxial loading conditions.

2) Square plate subjected to biaxial compressive loading

Next, a simply supported three-layer $(0^0/90^0/0^0)$ laminated square plate subjected

Tab. 2: The effect of E_1/E_2 ratios on the normalized critical buckling load for a simply supported four-layer $(0^0/90^0/90^0/0^0)$ square plate with a/h = 10.

Methods	E_1/E_2					
Methods	3	10	20	30	40	
RPIM-HSDT [46]	5.401	9.985	15.374	19.537	23.154	
IGA-TrSDTs [41]	5.3846	9.9120	15.2324	19.5654	23.1858	
IGA-FSDT [48]	5.3884	9.9303	15.2841	19.6558	23.3152	
FEM-HSDT [47]	5.114	9.774	15.298	19.957	23.340	
Elasticity [45]	5.294	9.762	15.019	19.304	22.881	
NSNI-HSDT [44]	5.4040	9.9628	15.3226	19.6901	23.3405	
Present	5.3855	9.9318	15.2814	19.6436	23.2908	

Tab. 3: The effect of a/h ratios on the normalized critical buckling load for a simply supported four-layer $(0^0/90^0/90^0/0^0)$ square plate with $E_1/E_2 = 40$.

Number players	Methods	a/h			
		10	20	50	100
$(0^0/90^0)$	MISQ20 [50]	11.169	12.520	12.967	13.033
	FEM-FSDT [49]	11.349	12.510	12.879	12.934
	FEM-FSDT [47]	11.353	12.515	12.884	12.939
	FEM-HSDT [47]	11.563	12.577	12.895	12.942
	IGA-FSDT [48]	11.097	12.4301	12.8724	12.9415
	Present	11.5101	12.5587	12.8911	12.9431
$(0^0/90^0/90^0/0^0)$	MISQ20 [50]	23.236	31.747	35.561	36.190
	FEM-FSDT [49]	23.409	31.625	35.254	35.851
	FEM-FSDT [47]	23.471	31.707	35.356	35.955
	FEM-HSDT [47]	23.349	31.637	35.419	35.971
	IGA-TrSDTs [41]	23.1858	31.6313	35.3458	35.9529
	NSNI-HSDT [44]	23.3405	31.7333	35.4808	36.1246
	IGA-FSDT [48]	23.1328	31.5511	35.3288	35.9566
	Present	23.2908	31.6365	35.3407	35.9571

to biaxial compressive loading is considered. A range of span-to-thickness ratios and elastic modulus ratios is investigated to assess their influence on the critical buckling factor. Tables 4 and 5 summarize the non-dimensional buckling loads for different cases. A comparison is made between the present results and established reference data which is reported by Fares and Zenkour [51], Khdeir and Librescu [52], Liu et al. [46], and Thai et al. [48] and Thai et al. [44] using NSNI. The comparisons show excellent agreement across all examined cases, further confirming the accuracy and reliability of the proposed methodology.

Tab. 4: The biaxial buckling behavior of a simply supported three-layer $(0^0/90^0/0^0)$ square plate for multiple E_1/E_2 ratios with a/h = 10.

	E_1/E_2			
Methods	10	20	30	40
FEM-FSDT [51]	4.963	7.588	8.575	10.202
FEM-HSDT [52]	4.963	7.516	9.056	10.259
IGA-FSDT [48]	4.9130	7.4408	8.7550	9.8795
NSNI-HSDT [44]	4.9278	7.45960	8.81694	8.81694
Present	4.9128	7.4401	8.7935	9.9291

Tab. 5: The biaxial buckling behavior of a simply supported three-layer $(0^0/90^0/0^0)$ square plate for multiple a/h ratios with $E_1/E_2 = 40$.

Methods	a/h					
Methods	2	5	10	15	20	
RPIM-HSDT [46]	1.457	5.519	10.251	12.239	13.164	
RPIM-FSDT [46]	1.419	5.484	10.189	10.189	13.132	
FEM-HSDT [52]	1.465	5.526	10.259	12.226	13.185	
IGA-FSDT [48]	1.4316	5.3236	9.8795	11.9978	13.0239	
NSNI-HSDT [46]	1.4540	5.3630	9.93146	12.08169	13.1309	
Present	1.4523	5.4185	9.9291	12.0219	13.0377	

4.2. Square plates designed with complex cutout geometries

To further verify the accuracy of the proposed approach, a simply supported three-layer square plate containing a central cutout is analyzed under uniaxial compressive loading. The material employed for the analysis is $E_1 = 2.45E_2$, $G_{12} =$ $0.48E_2$, $G_{23} = 0.2E_2$ and $\nu_{12} = 0.23$. The definition of the buckling load element is given by $\bar{\lambda} =$ $\lambda_{cr}/(\pi^2 D_0)$ in which $D_0 = E_1 h^3/12(1 - \nu_{12}\nu_{21})$. The geometry and nodal distribution are illustrated in Figure 4. Various angle-ply laminate configurations and side-to-thickness ratios are considered. For validation, the numerical outcomes are compared with those obtained by Yin et al. [53] using IGA based on CLP for thin plates, and with the NSNI-HSDT method [44]. In Table 6, the normalized buckling responses of a simply supported three-layer square plate with an intricate cutout are provided for both uniaxial and biaxial compression. Excellent agreement is observed across all examined side to thickness ratios and ply orientations. 5 depicts the buckling mode shapes of a simply support four-layer $(0^0/90^0/90^0/0^0)$ square plate with a/h = 10, $E_1/E_2 = 40$. The predicted mode shapes are consistent with physical expectations, further validating the effectiveness of the proposed method.

5. Conclusion

This study presented a novel Chebyshev Moving Kriging (CMK) meshfree method combined with the Third-Order Chebyshev Shear Deformation

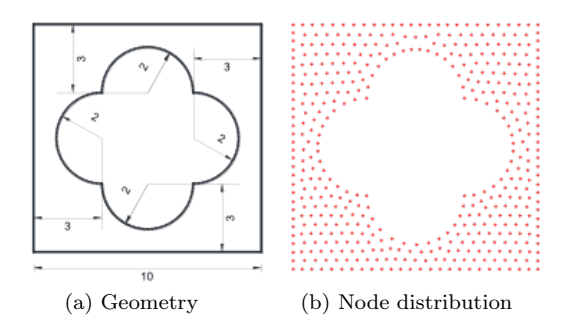


Fig. 4: Geometric configuration and nodal distribution of a square plate with a complex cutout.

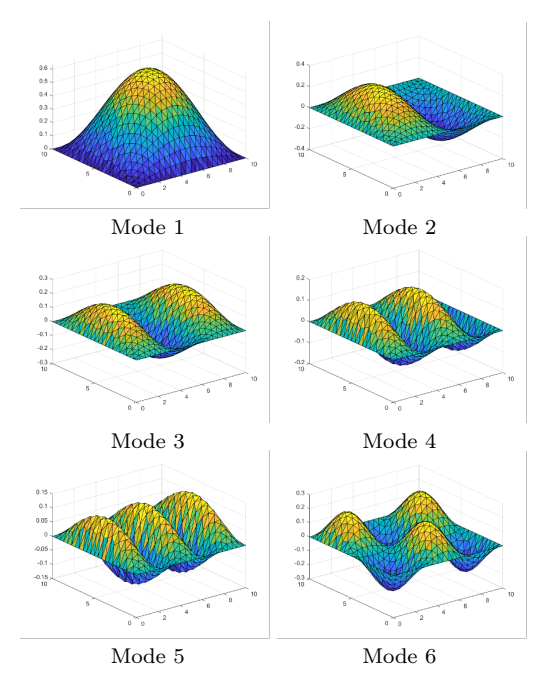


Fig. 5: Fundamental buckling modes of a simply support four-layer $(0^0/90^0/90^0/0^0)$ square plate with a/h = 10, $E_1/E_2 = 40$.

Theory (TCSDT) for the buckling analysis of laminated composite plates. By incorporating Chebyshev polynomials into both the interpolation functions and shear deformation formulation, the proposed framework achieves high accuracy, numerical stability, and computational efficiency.

From the numerical investigations, several important physical insights can be drawn:

• The normalized critical buckling load increases with a higher modulus ratio (E_1/E_2) , indicating that enhanced stiffness

a/h	Methods	Angled fiber layers					
a/n	Methods	(0/0/0)	(15/-15/15)	(30/-30/30)	(45/-45/45)	(0/90/0)	
Uniaxia	l compression						
166.67	IGA-CLPT [53]	1.360	1.479	1.715	1.827	1.359	
	NSNI-HSDT [44]	1.3560	1.4773	1.7180	1.8328	1.3547	
	Present	1.3617	1.4818	1.7195	1.8330	1.3610	
100	NSNI-HSDT [44]	1.3461	1.4661	1.7043	1.8186	1.3452	
	Present	1.3563	1.4752	1.7110	1.8242	1.3456	
10	NSNI-HSDT [44]	1.2098	1.3059	1.5059	1.6130	1.2200	
	Present	1.2138	1.3088		1.6165	1.2281	
5	NSNI-HSDT [44]	0.9894	1.0548	1.1927	1.2656	1.0084	
	Present	0.9876	1.0527	1.1909	1.2656	1.0148	
Biaxial	compression						
166.67	Present	0.6870	0.7542	0.8899	0.9584	0.6878	
100	Present	0.6853	0.7521	0.8870	0.9550	0.6863	
50	Present	0.6811	0.7469	0.8802	0.9476	0.6827	
10	Present	0.6342	0.6904	0.8082	0.8701	0.6397	
5	Present	0.5419	0.5839	0.6742	0.7229	0.5552	

Tab. 6: The effect of a complicated cutout on the normalized buckling load of a simply supported three-layer square plate.

in the fiber direction significantly improves the structural resistance against buckling.

- An increase in the span-to-thickness ratio (a/h) leads to higher normalized buckling factors, consistent with the expected mechanical behavior of laminated composites, where slender plates provide better buckling stability.
- For plates with complex cutouts and different fiber orientations, the proposed method captures realistic buckling responses and mode shapes, showing strong agreement with established benchmark results.

The main advantages of the proposed CMK–TCSDT approach can be summarized as follows:

- Accurate shear stress representation: The TCSDT inherently satisfies the zero-shear-stress condition at plate surfaces, eliminating the need for shear correction factors.
- Superior numerical stability: Chebyshev polynomials, due to their orthogonality and fast convergence, improve the robustness of the interpolation and reduce illconditioning compared to traditional polynomial functions.
- High versatility: The CMK framework allows meshfree modeling of both simple and

complex geometries, providing flexibility in handling laminated composite structures with arbitrary cutouts and boundary conditions.

Overall, the proposed methodology provides a reliable and efficient numerical tool for the buckling analysis of laminated composites. It not only reproduces benchmark solutions with excellent accuracy but also offers physical clarity and computational advantages, making it a promising approach for future studies of advanced material systems and structural configurations.

References

- [1] J.N Reddy. Mechanics of laminated composite plates and shells: theory and analysis. CRC press, 2003.
- [2] N.J. Pagano. Exact solutions for rectangular bidirectional composites and sandwich plates. J. Compos. Mater., 4(1):20–34, 1970.
- [3] A.K. Noor. Free vibrations of multilayered composite plates. AIAA J., 11(7):1038– 1039, 1973.
- [4] J.N. Reddy. A simple higher-order theory for laminated composite plates. J. Appl. Mech., 51(4):745-752, 1984.

- [5] N.D. Phan and J.N. Reddy. Analysis of laminated composite plates using a higherorder shear deformation theory. *Int. J. for Numer. Methods Eng.*, 21(12):2201–2219, 1985.
- [6] H. Nguyen-Xuan, T. Rabczuk, N. Nguyen-Thanh, T. Nguyen-Thoi, and S. Bordas. A node-based smoothed finite element method with stabilized discrete shear gap technique for analysis of reissner-mindlin plates. Comput. mechanics, 46:679-701, 2010.
- [7] M. Aydogdu. A new shear deformation theory for laminated composite plates. *Compos. structures*, 89(1):94–101, 2009.
- [8] S. Ambartsumian. On the theory of bending plates. *Izv Otd Tech Nauk AN SSSR*, 5(5):69–77, 1958.
- [9] P. Bose and J. Reddy. Analysis of composite plates using various plate theoriespart 1: Formulation and analytical solutions. Struct. engineering mechanics: An international journal, 6(6):583-612, 1998.
- [10] A. Ferreira, L.M. Castro, and S. Bertoluzza. A high order collocation method for the static and vibration analysis of composite plates using a first-order theory. *Compos.* structures, 89(3):424–432, 2009.
- [11] S.A. Ambartsumian. On the theory of bending of anisotropic plates and shallow shells. *J. Appl. Math. Mech.*, 24(2):500–514, 1960.
- [12] M. Levinson. An accurate, simple theory of the statics and dynamics of elastic plates. *Mech. Res. Commun.*, 7(6):343–350, 1980.
- [13] E. Reissner. On transverse bending of plates, including the effect of transverse shear deformation. *Int. J. Solids Struct.*, 11(5):569–573, 1975.
- [14] M. Stein. Nonlinear theory for plates and shells including the effects of transverse shearing. AIAA journal, 24(9):1537–1544, 1986.

- [15] M. Touratier. An efficient standard plate theory. *Int. J. Eng. Sci.*, 29(8):901–916, 1991.
- [16] K.P. Soldatos. A transverse shear deformation theory for homogeneous monoclinic plates. Acta Mech., 94(3):195–220, 1992.
- [17] N. Grover, B.N. Singh, and D.K. Maiti. New nonpolynomial shear-deformation theories for structural behavior of laminatedcomposite and sandwich plates. AIAA J., 51(8):1861–1871, 2013.
- [18] H. Arya, R.P. Shimpi, and N.K. Naik. A zigzag model for laminated composite beams. Compos. Struct., 56(1):21–24, 2002.
- [19] C.H. Thai, A.J.M. Ferreira, S.P.A. Bordas, T. Rabczuk, and H. Nguyen-Xuan. Isogeometric analysis of laminated composite and sandwich plates using a new inverse trigonometric shear deformation theory. Eur. J. Mech., 43:89–108, 2014.
- [20] J. Mantari, A. Oktem, and C.G. Soares. A new higher order shear deformation theory for sandwich and composite laminated plates. *Compos. Part B: Eng.*, 43(3):1489– 1499, 2012.
- [21] M. Karama, K. Afaq, and S. Mistou. Mechanical behaviour of laminated composite beam by the new multi-layered laminated composite structures model with transverse shear stress continuity. *Int. J. solids structures*, 40(6):1525–1546, 2003.
- [22] K. Soldatos. A transverse shear deformation theory for homogeneous monoclinic plates. Acta Mech., 94(3):195–220, 1992.
- [23] N.E. Meiche, A. Tounsi, N. Ziane, I. Mechab, and E.A.A. Bedia. A new hyperbolic shear deformation theory for buckling and vibration of functionally graded sandwich plate. *Int. J. Mech. Sci.*, 53(4):237–247, 2011.
- [24] S.S. Akavci and A.H. Tanrikulu. Buckling and free vibration analyses of laminated composite plates by using two new hyperbolic shear-deformation theories. *Mech. Compos. Mater.*, 44(2):145–154, 2008.

- [25] N. Grover, D.K. Maiti, and B.N. Singh. A new inverse hyperbolic shear deformation theory for static and buckling analysis of laminated composite and sandwich plates. *Compos. Struct.*, 95:667–675, 2013.
- [26] A. Mahi, E.A. Adda Bedia, and A. Tounsi. A new hyperbolic shear deformation theory for bending and free vibration analysis of isotropic, functionally graded, sandwich and laminated composite plates. Appl. Math. Model., 39(9):2489–2508, 2015.
- [27] L. Fox and I.B. Parker. Chebyshev polynomials in numerical analysis. Oxf. Math. Handbooks, 1968.
- [28] S.K. Jena, S. Chakraverty, and M. Malikan. Application of shifted chebyshev polynomial-based rayleigh-ritz method and navier's technique for vibration analysis of a functionally graded porous beam embedded in kerr foundation. Eng. with Comput., 37:3569–3589, 2021.
- [29] K. Lam, Q. Wang, and H. Li. A novel meshless approach—local kriging (lokriging) method with two-dimensional structural analysis. Comput. Mech., 33:235–244, 2004.
- [30] C.H. Thai, V.N.V. Do, and H. Nguyen-Xuan. An improved moving kriging-based meshfree method for static, dynamic and buckling analyses of functionally graded isotropic and sandwich plates. *Eng. Anal.* with Bound. Elem., 64:122–136, 2016.
- [31] C.H. Thai, T.N. Nguyen, T. Rabczuk, and H. Nguyen-Xuan. An improved moving kriging meshfree method for plate analysis using a refined plate theory. *Comput. & Struct.*, 176:34–49, 2016.
- [32] C.H. Thai, T. Tran, and P. Phung-Van. A size-dependent moving kriging meshfree model for deformation and free vibration analysis of functionally graded carbon nanotube-reinforced composite nanoplates. Eng. Anal. with Bound. Elem., 115:52–63, 2020.
- [33] C.H. Thai, A.J.M. Ferreira, J. Lee, and H. Nguyen-Xuan. An efficient sizedependent computational approach for

- functionally graded isotropic and sandwich microplates based on modified couple stress theory and moving kriging-based meshfree method. *Int. J. Mech. Sci.*, 142:322–338, 2018.
- [34] T.N. Nguyen, C.H. Thai, H. Nguyen-Xuan, and J. Lee. Geometrically nonlinear analysis of functionally graded material plates using an improved moving kriging meshfree method based on a refined plate theory. Compos. Struct., 193:268–280, 2018.
- [35] H. Li, Q. Wang, and K. Lam. Development of a novel meshless local kriging (lokriging) method for structural dynamic analysis. Comput. Methods Appl. Mech. Eng., 193(23-26):2599–2619, 2004.
- [36] L. Chen and K.M. Liew. A local petrovgalerkin approach with moving kriging interpolation for solving transient heat conduction problems. *Comput. Mech.*, 47:455– 467, 2011.
- [37] B. Dai, J. Cheng, and B. Zheng. A moving kriging interpolation-based meshless local petrov–galerkin method for elastodynamic analysis. *Int. J. Appl. Mech.*, 5(01):1350011, 2013.
- [38] C.H. Thai, A.J.M. Ferreira, H. Nguyen-Xuan, and P. Phung-Van. A size dependent meshfree model for functionally graded plates based on the nonlocal strain gradient theory. *Compos. Struct.*, 272:114169, 2021.
- [39] J.N. Reddy. A simple higher-order theory for laminated composite plates. *J. Appl. Mech.*, 51(4):745–752, 1984.
- [40] H. Nguyen-Xuan, C.H. Thai, and T. Nguyen-Thoi. Isogeometric finite element analysis of composite sandwich plates using a higher order shear deformation theory. *Compos. Part B: Eng.*, 55:558-574, 2013.
- [41] H. Arya, R. Shimpi, and N. Naik. A zigzag model for laminated composite beams. *Compos. structures*, 56(1):21–24, 2002.
- [42] J. Mantari, A. Oktem, and C.G. Soares. Static and dynamic analysis of laminated

- composite and sandwich plates and shells by using a new higher-order shear deformation theory. *Compos. structures*, 94(1):37–49, 2011.
- [43] C.H. Thai, S. Kulasegaram, L.V. Tran, and H. Nguyen-Xuan. Generalized shear deformation theory for functionally graded isotropic and sandwich plates based on isogeometric approach. *Comput. & Struct.*, 141:94–112, 2014.
- [44] C.H. Thai, A. Ferreira, and H. Nguyen-Xuan. Naturally stabilized nodal integration meshfree formulations for analysis of laminated composite and sandwich plates. *Compos. Struct.*, 178:260–276, 2017.
- [45] A. Noor and Mathers. Shear-flexible finite element method of laminated composite plate. Technical report, NASA, 1975.
- [46] L. Liu, L. Chua, and D. Ghista. Meshfree radial basis function method for static, free vibration and buckling analysis of shear deformable composite laminates. *Compos.* Struct., 78(1):58–69, 2007.
- [47] N. Phan and J. Reddy. Analysis of laminated composite plates using a higherorder shear deformation theory. Int. journal for numerical methods engineering, 21(12):2201–2219, 1985.
- [48] C.H. Thai, H. Nguyen-Xuan, N. Nguyen-Thanh, T.H. Le, T. Nguyen-Thoi, and T. Rabczuk. Static, free vibration, and buckling analysis of laminated composite reissner-mindlin plates using nurbs-based isogeometric approach. *Int. J. for Numer. Methods Eng.*, 91(6):571–603, 2012.
- [49] A. Chakrabarti and A. Sheikh. Buckling of laminated composite plates by a new element based on higher order shear deformation theory. *Mech. advanced Mater. Struct.*, 10(4):303–317, 2003.
- [50] H. Nguyen-Van, N. Mai-Duy, W. Karunasena, and T. Tran-Cong. Buckling and vibration analysis of laminated composite plate/shell structures via a smoothed quadrilateral flat shell

- element with in-plane rotations. Comput. & structures, 89(7-8):612-625, 2011.
- [51] M. Fares and A. Zenkour. Buckling and free vibration of non-homogeneous composite cross-ply laminated plates with various plate theories. *Compos. structures*, 44(4):279–287, 1999.
- [52] A. Khdeir and L. Librescu. Analysis of symmetric cross-ply laminated elastic plates using a higher-order theory: Part ii—buckling and free vibration. Compos. Struct., 9(4):259–277, 1988.
- [53] S. et al. Yin. A cutout isogeometric analysis for thin laminated composite plates using level sets. *Compos. Struct.*, 127:152–164, 2015.

About Authors

Lieu B. NGUYEN was born in Vietnam in 1984. She has a Ph.D. degree in Engineering Mechanics in 2019. Now, she is a lecturer at the Faculty of Civil Engineering, Ho Chi Minh City University of Technology and Education, Ho Chi Minh City, Vietnam. Her research interests are computational mechanics, and numerical methods for advanced materials